

Determination of scattering and Urbach absorption contributions to the light extinction in PTFE films by using graphical representation technique and numerical solution of the inverse problem

M.V. Sopinsky¹, K.P. Grytsenko^{1,2}, C. Villringer², Yu.V. Kolomzarov¹, S. Schrader²

¹V. Lashkaryov Institute of Semiconductor Physics, National Academy of Sciences of Ukraine, 41, prosp. Nauky, 03680 Kyiv, Ukraine

²Technical University of Applied Sciences Wildau (TH Wildau), Hochschulring 1, 15745 Wildau, Germany
Corresponding author e-mails: sopinsky@ua.fm, sopinsky@isp.kiev.ua

Abstract. Ellipsometrically obtained spectral dependences of ordinary α^{xy} and extraordinary α^z extinction/attenuation coefficients within the spectral range $\lambda = 300..980$ nm of uniaxially anisotropic polytetrafluoroethylene (PTFE) films were analyzed. We considered the capabilities and specific features of the graphical representation technique for determining the contribution of Rayleigh scattering and Urbach absorption to light attenuation in the spectral range beyond fundamental absorption. It has been shown that the graphical approach enables to estimate these contributions qualitatively, semi-quantitatively or quantitatively, depending on the situation. The conclusions made using the analysis of graphical representation are confirmed by numerical solution of the inverse problem *via* simulation of the $\alpha^{xy}(\lambda)$, $\alpha^z(\lambda)$ experimental dependences within the framework of a best-fit procedure. Being based on both of these approaches, we have ascertained that, in the as-prepared PTFE films, the so-called anomalous light scattering (ALS) with the spectral dependence of scattering coefficient $\alpha_s \approx a_s \lambda^{-p}$ ($p > 4$) takes place. Transformation of scattering from ALS to the Rayleigh one with $p \cong 4$ due to annealing is accompanied by an increase of Urbach (subband) absorption. Both of these factors cause narrowing the dynamic range of extinction coefficient values. Both scattering and absorption coefficients are higher for the component of light polarized along the normal to the substrate as compared to the component polarized in parallel to it. The relationship between observed behavior of the scattering and absorption coefficients and the film structure has been discussed.

Keywords: Rayleigh scattering, Urbach tail, absorption coefficient, scattering coefficient, graphical method, ellipsometry, polytetrafluoroethylene.

<https://doi.org/10.15407/spqeo26.03.303>

PACS 42.25.Bs, Fx, 42.70.Jk, 42.79.Wc, 78.20.Fm, 78.40.Ha, Pg, 78.66.Nk, Qn, 81.70.Fy

Manuscript received 20.03.23; revised version received 22.08.23; accepted for publication 13.09.23; published online 20.09.23.

1. Introduction

The distinction between absorption and scattering in the spectral range beyond fundamental absorption is important for characterization of practical properties of any optical material. As an inelastic process, absorption not only attenuates transmitted light but also transforms it into heat. This can lead to the overheating and degradation of material, causing problems especially in high power applications [1, 2]. In contrast, scattering causes negligible internal energy transfer, because it essentially involves elastic processes. Nevertheless, it is undesirable in many applications [1–4]. In addition, obtaining data on the nature of optical losses in the

spectral range beyond fundamental absorption can provide essential information for analyzing the structure of a material and finding ways to purposefully change it. Thus, information about the contributions of absorption and scattering to the attenuation of light in this spectral region of the material is important from both fundamental and practical viewpoints.

This work is aimed at determining the contribution and type of scattering and absorption as based on the analysis of the extinction coefficient spectra. A series of samples of polytetrafluoroethylene (PTFE) film, the practically important material [5], was analyzed. The band gap E_g for different types of PTFE samples was found to be within the 5...10 eV interval [6–9] which

corresponds to the middle and far ultraviolet spectral regions. Our measurements of extinction coefficient were performed in near infrared, visible, and near ultraviolet spectral ranges. The results for two PTFE films, prepared using two different technological ways and, as a result, having different optical characteristics, are presented.

'Try graphics first' is one of basic scientific principles when analyzing the data in many research areas [10]. The graphical representation technique is widely used for analyzing the data on scattering or absorption. However, we did not find works where this method was used to separate the contributions of scattering and absorption to the total extinction coefficient. This work is intended to fill this gap. Considerable attention is paid to methodological aspects of using the graphical representation technique in this case. First, the possibilities of the technique for express estimation of the scattering and subband absorption contributions to light extinction were estimated. It was shown that this simple graphical approach enables to estimate these contributions qualitatively, semi-quantitatively, or quantitatively, depending on the situation. It is also shown that graphical analysis is important to form an adequate parametric model in the numerical solution of the inverse problem (IP). Also, it allows us to obtain a reasonable initial approximation of the model's parameters that significantly simplifies the numerical solution of IP. Solving IP was performed using simulation of experimental dependences of extinction coefficients within the framework of a best-fit procedure. The IP solutions confirmed the conclusions of the graphical technique.

2. Experimental

The 1.0- μm thick PTFE film No 16 was prepared using the method of evaporation-activation of PTFE in a high vacuum (the so-called electron-enhanced vacuum deposition (EVD) [6]) at the pressure of active fluorinated volatile fragments $2 \cdot 10^{-4}$ mbar. The 0.5- μm thick PTFE film No 28 was prepared using the EVD method with additional non-self-sustained radio frequency plasma at comparatively low pressure and power ($9 \cdot 10^{-4}$ mbar, 50 W) in fluoropolymer gas fragments (for details of this technology, see reference [11]). The films were deposited on polished slides of monocrystalline silicon at the ambient temperature. Ellipsometry is a versatile and sensitive method for studying various characteristics of materials [12–15]. SENresearch SE 800 DUV ellipsometer (Sentech Instruments, Berlin-Adlershof, Germany) and SpectraRay/4 – SENTECH comprehensive software for spectral ellipsometry data acquisition and analysis were used. The obtained spectral dependences of refractive indices are presented in Fig. 1. They show that the films are uniaxially anisotropic with an optical axis perpendicular to the substrate plane. The values of ordinary n^{xy} , k^{xy} and extraordinary n^z , k^z refractive and extinction indices were determined at 150 measured points within $\lambda = 300 \dots 980$ nm spectral range. At $\lambda = 632.8$ nm,

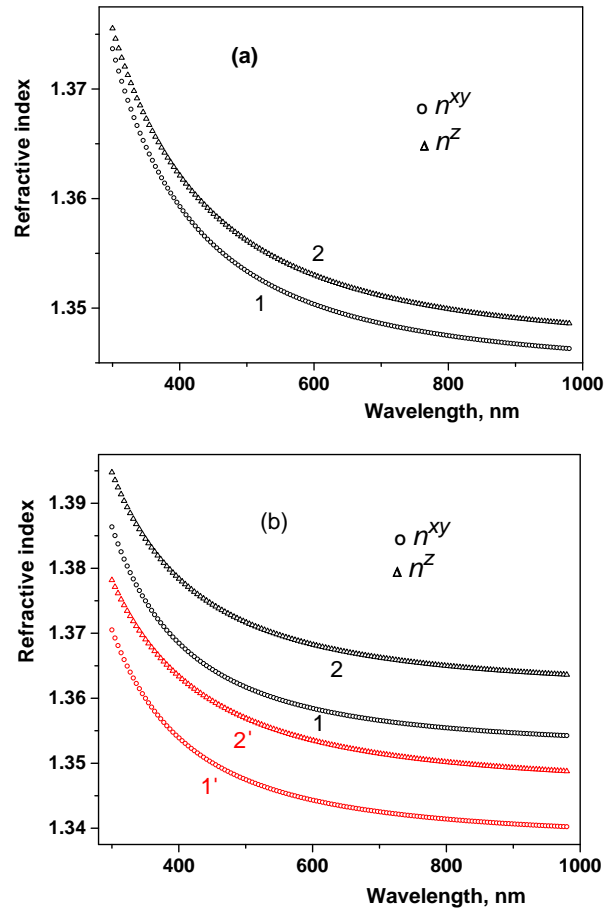


Fig. 1. Spectral dependences for the ordinary n^{xy} (I, I') and extraordinary n^z ($2, 2'$) refractive indexes of the films No 16 (a) and No 28 (b). $I, 2$ – for the as-deposited films, $I', 2'$ – for the film No 28 after annealing in Thermo Scientific Cimarec oven at 80 °C for 1 h in nitrogen atmosphere.

the values of ordinary n^{xy} and extraordinary n^z refractive indices are as follows: for the film No 16 $n^{xy} = 1.3496$, $n^z = 1.3523$ ($n^z - n^{xy} = 0.0027$), for the film No 28 $n^{xy} = 1.3577$, $n^z = 1.3675$ ($n^z - n^{xy} = 0.0098$). After the one-hour annealing at 80 °C in nitrogen atmosphere, the refractive indexes of the film No 28 reached the values: $n^{xy} = 1.3436$, $n^z = 1.3527$ ($n^z - n^{xy} = 0.0091$).

3. Possible mechanisms of scattering and absorption in the “transparency range” and their identification by using the graphical analysis of the extinction coefficient experimental dependence

When a light beam propagates in any medium, its intensity gets attenuated to a certain extent in accord to the law

$$I(z) = I_0 \exp(-\alpha d). \quad (1)$$

When the light beam passes through the medium, both absorption and scattering can contribute to attenuation [1–4]:

$$\alpha = \alpha_a + \alpha_s, \quad (2)$$

where α_a is the absorption coefficient and α_s is the scattering coefficient.

Scattering losses may be caused by any of several contributing factors. The first is Rayleigh scattering on the much-smaller-than-wavelength inhomogeneities inside the solid that cause fluctuations of the refractive index. Another important aspect of Rayleigh scattering is the assumption that particles are randomly spaced, resulting in the scattered light being incoherent [3, 4]. Spectral behavior of Rayleigh scattering has the form [1–4]:

$$\alpha_s = a_R / \lambda^4, \quad (3)$$

where a_R is the Rayleigh coefficient characterizing the scattering efficiency in a given sample. This dependence has been observed experimentally numerous times. With increase of inhomogeneities' dimensions (dimensions of scattering particles) the $\alpha_s \sim \lambda^{-p}$ dependence with $p < 4$ takes place (Mie scattering) [16, 17]. The larger the particle size, the smaller the exponent.

Generally speaking, the fulfillment of power dependence in the form of $\alpha \approx a\lambda^{-p}$ in any case is a proof of the dominance of scattering [3, 4]. In nanostructured glasses (phase-separated glasses, glass-ceramics) anomalous light scattering (ALS) [3, 4, 17] with $p > 4$ is observed. There were a few papers that considered the ALS problem in detail. It is known that shape, orientation, polydispersity of inclusions, and their distinct refractive indices influence the degree of light scattered due to ALS [3, 4, 17]. Thus, for the wavelength-dependent scattering we can generally write:

$$\alpha_s = a_s / \lambda^p \quad (4)$$

or the same

$$\alpha_s = A_s (h\nu)^p, \quad (5)$$

where $a_s(A_s)$ is the coefficient of wavelength-dependent scattering.

The scattering component caused by the surface roughness σ in our films can be estimated using the following formula [18] $\alpha_{ds} = R_0 \exp\left[-(4\pi\sigma)^2 / \lambda^2\right]$, where R_0 is the reflection coefficient of the specularly reflected light. At a surface roughness of $\sim 2 \dots 3$ nm, the contribution of surface scattering to the reflectance is less than 1% [18]. Thus, surface scattering is neglected in further consideration. Manufacturing-related light loss caused by macrodefects (macro-imperfections) that exceed the probe wavelength can also contribute to the extinction coefficient. This component is wavelength-independent.

In low crystalline, poor crystalline, disordered and amorphous materials, an exponential part of the absorption coefficient energy spectrum beyond the optical band edge (Urbach tail) is observed [19]:

$$\alpha_a = \alpha_0 \exp(h\nu/E_U). \quad (6)$$

This type of absorption occurs, because these materials have localized states that extend into the band gap. Urbach energy E_U is often interpreted as the band tail width due to the localized band gap states.

Graphical representation technique is widely used to determine both the scattering characteristics and the characteristics of subband absorption. To detect the exponential section in the $\alpha(h\nu)$ dependence, the ordinata is plotted in a logarithmic scale. The value of Urbach energy is determined from the inverse of the slope of the $\ln\alpha - h\nu$ curve's linear portion. Most papers that study near-edge absorption don't account for the contribution of scattering into the extinction coefficient, which introduces an additional error into the determined E_U value.

In turn, in case of domination of scattering, plotting experimental data in $\ln\alpha - \ln\lambda$ or $\ln\alpha - \ln h\nu$ coordinates is the simplest and quickest way to determine the type of scattering (Mie, Rayleigh or ALS) and the exact values of the parameters $a_s(A_s)$, p . As $\ln\alpha_s = \ln A_s + p \ln h\nu$, the slope of this line gives the p value, and the scattering constant value is determined from the equation $\ln A_s = -p \ln h\nu_1$, where $h\nu_1$ is the photon energy, for which $\alpha_s = 1$ in the units of the α_s measurement.

In the case of noticeable contribution from wavelength-independent scattering, that is

$$\alpha_s = a_s \lambda^{-p} + b_s \quad (7)$$

or the same

$$\alpha_s = A_s (h\nu)^p + B_s, \quad (8)$$

plotting the experimental curve in double logarithmic coordinates will no longer give the exact values of A_s and p , because in this case

$$\ln\alpha_s = \ln A_s + p \ln(h\nu) + \ln\left[1 + (B_s/A_s)(h\nu)^{-p}\right]. \quad (9)$$

The presence of λ -independent component in scattering will distort the long-wave part of the $\ln a_s(\ln h\nu)$ spectral dependences to a higher degree. Therefore, the short-wave part of this plot gives better estimate of the A_s and p values. The exact values of the parameters p , $a_s(A_s)$, $b_s(B_s)$ can be obtained by plotting the experimental plots $\alpha(\lambda)$ or $\alpha(h\nu)$ in the $\alpha - \lambda^{-p}$ or $\alpha - (h\nu)^p$ coordinates and choosing the value of p that gives the best linear approximation. In essence, this is a graphical finding of the inverse problem exact solution within the framework of a model that takes into account both the λ -dependent and λ -independent components of scattering. For example, this is how the values of the Rayleigh constant a_R and the λ -independent constant b_s were obtained from the linear dependence $\alpha(\lambda)$ in the $\alpha - \lambda^{-4}$ coordinates in the pure GeO_2 core-F-doped GeO_2 cladding fiber [20]. The b_s/a_R relation was found to be ~ 3.6 . In [21] for the fluoride-glass optical fibers the linear dependence was found in $\alpha - \lambda^{-2.4}$ coordinates with the b_s/a_s ratio of 0.1.

3.1. Analysis of extinction coefficient experimental dependences by using the graphical representation technique and numerical solution of the inverse problem

In this analysis, we use not the wavelength scale, as it is usually accepted in the analysis of scattering spectra, but photon energy scale, as is customary in the analysis of absorption spectra.

3.1.1. $\alpha^{xy}(hv)$ and $\alpha^z(hv)$ dependences of the film 16

For the film 16, since the wavelength decreases from 980 nm ($hv = 1.2653$ eV) to 300 nm ($hv = 4.1333$ eV), the extinction coefficient α^{xy} for the component of the light polarized in the directions parallel to substrate increases by a factor of 372: from 0.022 to 8.27 cm^{-1} . For the component of the light polarized along the normal to substrate, the extinction coefficient α^z is more than an order of magnitude larger. When λ is decreased from 980 to 300 nm, α^z increases 237 times from 0.70 to 166.0 cm^{-1} . The α^z growth in relation to the α^{xy} is more pronounced in the long-wave part of the spectrum: at $\lambda = 300$ nm $\alpha^z/\alpha^{xy} \cong 20$, at $\lambda = 980$ nm $\alpha^z/\alpha^{xy} \cong 32$.

Fig. 2 shows $\alpha^{xy}(hv)$ and $\alpha^z(hv)$ experimental plots in double logarithmic and semi-logarithmic coordinates. As can be seen, in $\ln - \ln$ coordinates they are close to linear, and in semi-log coordinates have a sublinear appearance. Thus, representation of the experimental curves in these coordinates indicates that the light scattering determines the spectral behavior of the α^{xy} and α^z extinction coefficients. By connecting endpoints on plots (1) and (2) of Fig. 2a by straight lines, we get the estimated values of the parameter p : 4.62 for the polarization normal to substrate (z -polarization direction) and 5.00 for the polarization parallel to substrate (xy -polarization directions). Since $p > 4$, then the scattering is anomalous. To more accurately determine the values of the parameters that define the course of the spectral dependences α^{xy} , α^z by the graphical method, we performed a linear approximation of the experimental spectral plots $\alpha^{xy}(hv)$, $\alpha^z(hv)$ in various coordinates by using the option "Analysis \rightarrow Fit Linear" from the Origin 6.1 software package (OriginLab Corporation). This option performs linear regression analysis by the ordinary least squares method (OLSM).

The $\alpha^{xy}(hv)$ experimental plot of the film 16 in $\ln \alpha^{xy} - \ln hv$ coordinates is ideally described by the linear fit $\ln \alpha^{xy} = -4.98(\pm 1.2 \cdot 10^{-5}) + 5.00(\pm 1.52 \cdot 10^{-5}) \ln hv$ ($R = 1$, $SD = 6.0 \cdot 10^{-6}$, where R is the square root of coefficient of determination, and SD is residual standard deviation, $hv_1 = 2.707$ eV, $A_s = 6.86 \cdot 10^{-3} \text{ cm}^{-1}$). In $\alpha^{xy} - (hv)^5$ coordinates, the experimental plot $\alpha^{xy}(hv)$ is ideally described by the line $\alpha^{xy} = [6.86 \cdot 10^{-3} (\pm 3.28 \cdot 10^{-9}) \text{ cm}^{-1}] (hv)^5 - 8.33 \cdot 10^{-7} (\pm 9.04 \cdot 10^{-7}) \text{ cm}^{-1}$ ($R = 1$, $SD = 9.65 \cdot 10^{-6} \text{ cm}^{-1}$). Thus, using this graphical representation technique analysis, we may definitely conclude that, within the

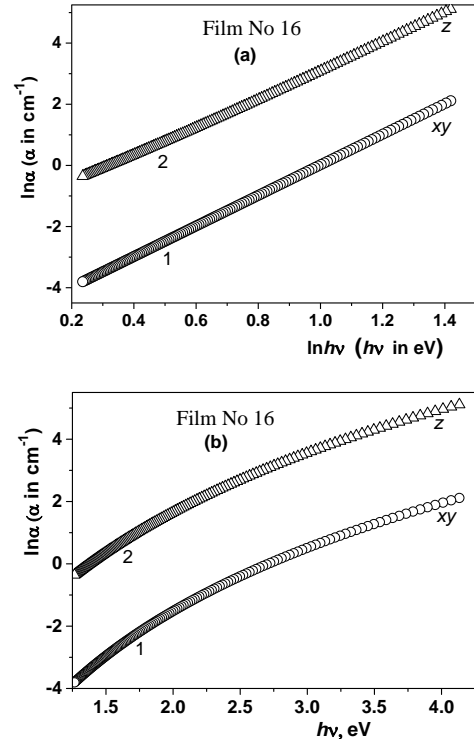


Fig. 2. Spectral dependences of α^{xy} (1) and α^z (2) in $\ln \alpha - \ln hv$ (a) and $\ln \alpha - hv$ (b) coordinates for the film No 16.

spectral range 300 to 980 nm, the extinction coefficient α^{xy} in the film 16 is defined by ALS with $p = 5.00$ and $A_s = 6.86 \cdot 10^{-3} \text{ cm}^{-1}$. This is proved by the fact that the set of 150 experimental points (hv_i, α^{xy}_i) is approximated by dependence (9) with the almost zero value of B_s and standard error of A_s , which is six orders of magnitude less than A_s .

The linear fit of the $\alpha^z(hv)$ experimental plot in $\ln - \ln$ coordinates is somewhat less ideal than for the $\alpha^{xy}(hv)$ plot: $\ln \alpha^z = -1.50(\pm 0.0596) + 4.61(\pm 0.00757) \ln hv$ ($R = 0.9998$, $SD = 0.03085$, $A_s = 0.223 \text{ cm}^{-1}$, $hv_1 = 0.697$ eV). Linear fit in $\alpha^z - (hv)^{4.61}$ coordinates gives: $R = 0.9997$, $SD = 0.815 \text{ cm}^{-1}$ at $A_s = 0.2347 \text{ cm}^{-1}$ and $B_s = \alpha^z(hv = 0) = -0.5744 \text{ cm}^{-1}$. Thus, the graphic analysis shows that the model of wavelength-dependent scattering with two parameters, A_s and p , does not quite perfectly describe the spectral course of α^z , as it is evidenced by the negative value of α^z at $hv = 0$. The value $p = 4.61$ is the lower estimate of the parameter p . A more accurate lower estimate of p can be obtained, for example, by the linear fit in the range $\alpha^z \geq 1.0$. For this range $\ln \alpha^z = -1.74 + 4.8244 \ln hv$ ($R = 0.99999$, $A_s = 0.1755 \text{ cm}^{-1}$, $hv_1 = 0.722$ eV). By plotting the $\alpha^z(hv)$ experimental dependences in the coordinates $\alpha^z - (hv)^p$, it was found that the best linear approximation of the entire measured range is achieved in the $\alpha^z - (hv)^{4.853}$ coordinates: $R = 1$, $SD = 0.084 \text{ cm}^{-1}$ at $A_s = 0.169 \pm 3.5 \cdot 10^{-5} \text{ cm}^{-1}$, $B_s = \alpha^z(hv = 0) = 0.2906 \pm 7.92 \cdot 10^{-3} \text{ cm}^{-1}$, $B_s/A_s = 1.72$. In fact, this is a graphical solution of the

inverse problem within the framework of the model described by the equation (8). Thus, taking into account the λ -independent scattering component increases the exponent of the λ -dependent component from 4.61 to 4.853.

It can be seen that the expression (8) describes the spectral course of the extinction coefficient for the component of light polarized in the directions perpendicular to substrate worse than for the component of the light polarized in the directions parallel to substrate. In the former case, the relative error of parameter A_s is $2.1 \cdot 10^{-2}\%$, while in the latter case $4.8 \cdot 10^{-5}\%$. A relatively large value of the B_s/A_s ratio stands out, as well as the fact that the relative error in determining B_s (2.8%) is two orders of magnitude higher than the error in determining A_s . This may indicate that deviation from the strict power dependence is mainly caused not by the presence of λ -independent scattering, but by the presence of defect absorption. To test this assumption, a comparative numerical solution of IP was carried out using two goal functions:

$$G_1 = \sum [A_s (hv_i)^p + B_s - \alpha_i^{\text{exp}}]^2, \quad (10)$$

and

$$G_2 = \sum [A_s (hv_i)^p + \alpha_0 \exp(hv_i/E_U) - \alpha_i^{\text{exp}}]^2. \quad (11)$$

Solution of IP consisted of finding the values of the parameters A_s , B_s , p , α_0 and E_U , that provide the minimum of the goal functions G_1 or G_2 . The estimated values obtained by the graphical method served as the initial values of the variable parameters in the numerical minimization. The summation was carried out over all 150 points at which the extinction coefficient was determined.

In the case of solving IP in the frame of model (8), minimization of G_1 is identical to the performance of linear regression analysis by OLSM. Indeed, for z -direction $G_1^{\text{min}} = 1.0584 \text{ cm}^{-2}$ at $A_s = 0.1689 \text{ cm}^{-1}$, $B_s = 0.291 \text{ cm}^{-1}$, $p = 4.853$ is obtained. Thereof, $(G_1^{\text{min}}/150)^{1/2} = 0.084$, which is equal to the SD value obtained by linear regression in $\alpha^z - (hv)^{4.853}$ coordinates. At the same time, $G_2^{\text{min}} = 0.03875 \text{ cm}^{-2}$ (27 times less than G_1^{min}) at $A_s = 0.162 \text{ cm}^{-1}$, $p = 4.833$, $\alpha_0 = 0.0384 \text{ cm}^{-1}$, $E_U = 0.72 \text{ eV}$. Comparison of G_1^{min} and G_2^{min} points out that the main role in deviation of experimental $\alpha^z(hv)$ plot from pure power dependence is mainly caused by the Urbach absorption. This conclusion is also confirmed by the fact that minimization within the goal function

$$G_3 = \sum [A_s (hv_i)^p + \alpha_0 \cdot \exp(hv_i/E_U) + B_s - \alpha_i^{\text{exp}}]^2 \quad (12)$$

only slightly (by 8%) reduces the error, and for B_s the value close to zero (-0.03 cm^{-1}) is obtained. Wherein, the p and E_U values practically was not changed, the A_s value decreased by 6%, and the value of E_U increased by 10%.

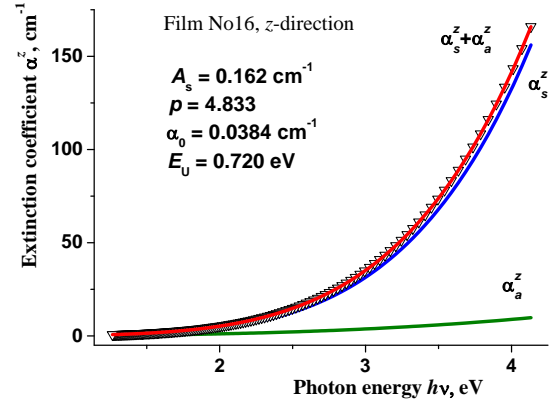


Fig. 3. α^z spectral dependence (triangles) as well as its simulation with the sum (red curve $\alpha_s^z + \alpha_a^z$) of absorption (green curve α_a^z) and scattering (blue curve α_s^z) components for the film 16. The minimization parameters are shown in the figure.

The fitting results for $\alpha^z(hv)$ dependence corresponding to minimum of G_2 are shown in Fig. 3. For the z -direction, the relation of absorption to scattering coefficients decreases from 0.442 to 0.0775, since the wavelength decreases from 980 down to 300 nm. Thus, the relative contribution of absorption is higher in the long-wave part of the spectrum. This is analogous to how the presence of λ -independent scattering manifests itself in the sense of influencing the shape of the spectrum. Note that, in the spectral range $hv \sim E_U$, the contribution of the Urbach absorption will change very little with a change in the wavelength, *i.e.*, behavior of the term $\alpha_0 \exp(hv/E_U)$ in terms of the contribution to the spectral course of the extinction coefficient will be a little different from the contribution of the term B_s with a value close to that of $\alpha_0 \cdot e$.

3.1.2. $\alpha^{xy}(hv)$ dependences for the film 28 before and after annealing

Fig. 4 shows the plots of $\alpha^{xy}(hv)$ spectral dependences in $\ln \alpha^{xy} - \ln hv$ and $\ln \alpha^{xy} - hv$ coordinates for the as-deposited film 28 (curves 1) and for this film after the one-hour annealing at 80 °C in nitrogen atmosphere (curves 2). As the wavelength decreases from 980 down to 300 nm, the extinction coefficient for the component of the light polarized in the directions parallel to substrate in the as-deposited film 28 monotonically increases by a factor of 360 from 2.5 to 900.0 cm^{-1} . *I.e.*, the dynamic range of the α^{xy} values in the films 16 and 28 is practically the same, although the α^{xy} values themselves differ by two orders of magnitude. The annealing leads to an increase in α^{xy} over the entire range; this growth is more pronounced in the long-wave part of the spectrum. As a result, the dynamic range of the α^{xy} values decreases: α^{xy} increases seventy-fold from 15.5 cm^{-1} at $\lambda = 980 \text{ nm}$ up to 1106 cm^{-1} at $\lambda = 300 \text{ nm}$.

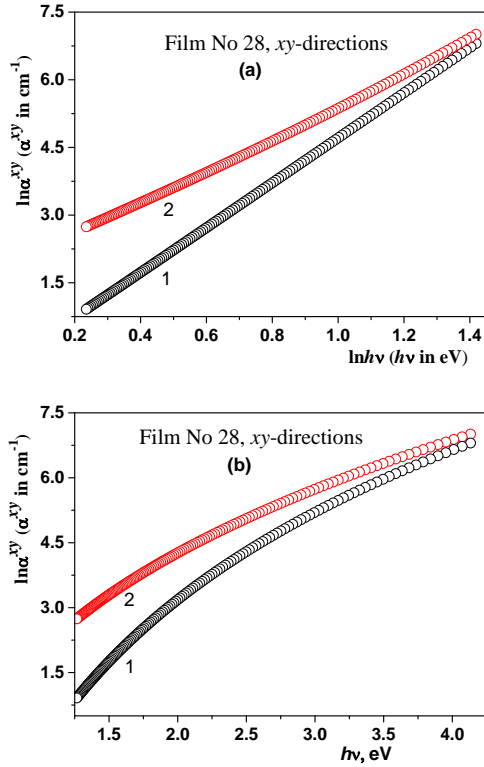


Fig. 4. α^{xy} spectral dependences in $\ln\alpha^{xy} - \ln hv$ (a) and $\ln\alpha^{xy} - hv$ (b) coordinates for the as-deposited film 28 (1) and for this film after one-hour annealing at 80 °C in nitrogen atmosphere (2).

It can be seen from the figure that, as in the case of the $\alpha^{xy}(hv)$ dependence for the film 16, the $\alpha^{xy}(hv)$ dependence in the film 28 in $\ln\alpha^{xy} - \ln hv$ coordinates is close to linear both before and after annealing, while in $\ln\alpha^{xy} - hv$ coordinates it has a sublinear form. That is, light scattering plays a determining role in the spectral behavior of α^{xy} for the film 28 as well.

Compared to the as-deposited film 16, the linear fit in $\ln - \ln$ coordinates describes the experimental plot $\alpha^{xy}(hv)$ of the as-deposited film 28 slightly less ideally: $\ln\alpha^{xy} = -0.263 + 4.975\ln hv$ ($R = 1$, $SD = 0.00244$), $hv_1 = 1.054$ eV. In $\alpha^{xy} - (hv)^{4.975}$ coordinates, linear approximation gives $\alpha^{xy} = -0.209 \text{ cm}^{-1} + 0.772(hv)^{4.975} \text{ cm}^{-1}$ ($R = 1$, $SD = 0.00305 \text{ cm}^{-1}$). The negative value $B_s = -0.209 \text{ cm}^{-1}$ at $p = 4.975$ indicates that description of experimental data by the dependence (5) is not fully adequate. Selection of p values in the framework of the model (8) shows that the best linear approximation is achieved in the $\alpha^{xy} - (hv)^{4.992}$ coordinates: $R = 1$, $SD = 0.02577 \text{ cm}^{-1}$ at $A_s = 0.7543 \pm 8.9 \cdot 10^{-8} \text{ cm}^{-1}$, $B_s = 0.0865 \pm 2.4 \cdot 10^{-3} \text{ cm}^{-1}$ ($B_s/A_s = 0.115$). Thus, the exponent value for the λ -dependent part of the scattering for xy -polarization directions in the as-deposited films 28 and 16 completely agrees, as well as the accuracy of description with the dependence (8). The difference is a very small increase of the λ -independent contribution in the $\alpha^{xy}(hv)$ plot for the film 28.

After annealing, the α^{xy} values for the film 28 increase over the entire measured range. As already noted, a stronger relative increase in α^{xy} takes place in the long-wave part of the range. This leads to a narrowing of the α^{xy} dynamic range. From (5), (6) and (8), it follows that this narrowing can be caused by a decrease in the parameter p and an increase in the parameters B_s , E_U . In the first approximation, the dependence $\alpha^{xy}(hv)$ in $\ln - \ln$ coordinates can be considered linear with a slope smaller than that before annealing. However, it is even visually seen that, after annealing, description with a purely power dependence worsens: the slope of the $\alpha^{xy}(hv)$ plot in $\ln - \ln$ coordinates is smaller at the lower photon energies. Naturally, this also manifests itself in the linear approximation in these coordinates for which $R = 0.99942$, $SD = 0.04045$, $\ln\alpha^{xy} = 1.08408 + 3.555\ln hv$ ($hv_1 = 0.737$ eV). A linear fit in $\alpha^{xy} - (hv)^{3.555}$ coordinates shows very poor accuracy ($R = 0.99866$, $SD = 12.0 \text{ cm}^{-1}$) and negative $B_s = -8.994 \text{ cm}^{-1}$. By selection, it was found that the best description in the $\alpha^{xy} - (hv)^p$ coordinates is achieved at $p = 4.00$. At the same time $A_s = 3.726 \pm 3.1 \cdot 10^{-3} \text{ cm}^{-1}$, $B_s = 9.251 \pm 2.32 \cdot 10^{-1} \text{ cm}^{-1}$ ($B_s/A_s = 2.48$), $R = 0.99995$, $SD = 2.35 \text{ cm}^{-1}$.

It follows from the graphical analysis of the $\alpha^{xy}(hv)$ plots before and after annealing in the framework of the model (9) that, on the one hand, the annealing leads to the transition from the ALS to the Rayleigh-type scattering. And, on the other hand, it leads to a more significant growth of λ -independent components of scattering: if A_s grows five times, then B_s grows more than hundred times. This is accompanied by a significant increase in the relative error of determining A_s – it increases from $1.2 \cdot 10^{-3}\%$ to $8.3 \cdot 10^{-2}\%$. All this suggests that such a deterioration in description with the model (8) is caused by the appearance of the Urbach absorption. This assumption is confirmed by lower sublinearity of curve 2 in Fig. 4b and minimization results of G_1 and G_2 :

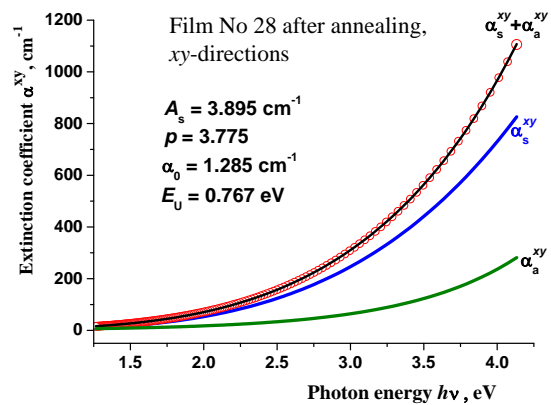


Fig. 5. α^{xy} spectral dependence (circles) as well as its simulation with the sum (black curve $\alpha_s^{xy} + \alpha_a^{xy}$) of absorption (green curve α_a^{xy}) and scattering (blue curve α_s^{xy}) components for the film 28 after one-hour annealing at 80 °C in nitrogen atmosphere. The minimization parameters are shown in the figure.

$G_1^{\min} = 828.4 \text{ cm}^{-2}$; $G_2^{\min} = 22.8 \text{ cm}^{-2}$ (36 times less than G_1^{\min}) at $A_s = 3.895 \text{ cm}^{-1}$, $p = 3.775$, $\alpha_0 = 1.285 \text{ cm}^{-1}$, $E_U = 0.767 \text{ eV}$. The fitting results corresponding to the G_2 minimum are shown in Fig. 5. The decrease of p as a result of annealing from ≈ 4.99 down to ≈ 3.88 indicates the destruction of an ordered placement of the scattering centers in the directions parallel to substrate. Due to this, after annealing the scattering in the long-wave part of the spectrum increases, and decreases in the short-wave region. For example, after annealing $\alpha_s^{xy}(980 \text{ nm}) = 9.5 \text{ cm}^{-1}$, $\alpha_s^{xy}(300 \text{ nm}) = 826 \text{ cm}^{-1}$, whereas before annealing $\alpha_s^{xy}(980 \text{ nm}) \cong 2.5 \text{ cm}^{-1}$, $\alpha_s^{xy}(300 \text{ nm}) \cong 900 \text{ cm}^{-1}$. The growth of α^{xy} in the entire spectral range due to annealing is a consequence of the appearance of the Urbach absorption. The relation $\alpha_a^{xy}/\alpha_s^{xy}$ is 0.70 at 980 nm and 0.34 at 300 nm. *I.e.*, the relative contribution of the absorption is higher in the long-wave range.

3.1.3. $\alpha^z(h\nu)$ dependences for the film 28 before and after annealing

The plots of $\alpha^z(h\nu)$ spectral dependences for the film 28 in the double logarithmic and semi-log Urbach coordinates before (curves 1) and after (curves 2) annealing at 80°C are shown in Fig. 6. In $\ln - \ln$ coordinates (Fig. 6a), these plots are superlinear. In semi-log coordinates (Fig. 6b) the plot for the as-prepared film also exhibits superlinearity that is much smaller than that in $\ln - \ln$ coordinates. The plot for the annealed film is slightly sublinear. From these graphical representations, we can conclude that, for z -polarization direction, the Urbach absorption provides prevailing contribution to the extinction coefficient of the film 28 both before and after annealing, with its dominance being more pronounced in the annealed film. As

$$\ln \alpha = \ln \alpha_0 + h\nu/E_U + \ln \left\{ 1 + (A_s/\alpha_0) \left[(h\nu)^p / \exp(h\nu/E_U) \right] \right\}, \quad (13)$$

then superlinearity is observed when the value $[(h\nu)^p / \exp(h\nu/E_U)]$ increases with increasing the photon energy, *i.e.*, $(h\nu)^p$ grows faster than $\exp(h\nu/E_U)$. Conversely, when this value decreases with the increase in $h\nu$, there will be a deviation from straight line towards sublinearity. The first case corresponds to the larger values of p and/or E_U , while the second one, on the contrary, to the smaller values of p and/or E_U . Thus, in the case of a significant contribution of the Urbach absorption, the shape of the graph $\alpha(h\nu)$ in semi-logarithmic coordinates can provide semi-quantitative information about the parameters p and E_U . As far as physics goes, knowledge of these parameters is a most important.

When the wavelength decreases from 980 to 300 nm, the extinction coefficient α^z increases from 134 to 2357 cm^{-1} in the as-prepared film, and from 150 to 2320 cm^{-1} in the annealed film. In the long-wave range, annealing leads to some increase in α^z . At the short-wave edge of the measured spectrum, α^z even decreases after annealing. Therefore, the ratio of the maximum and

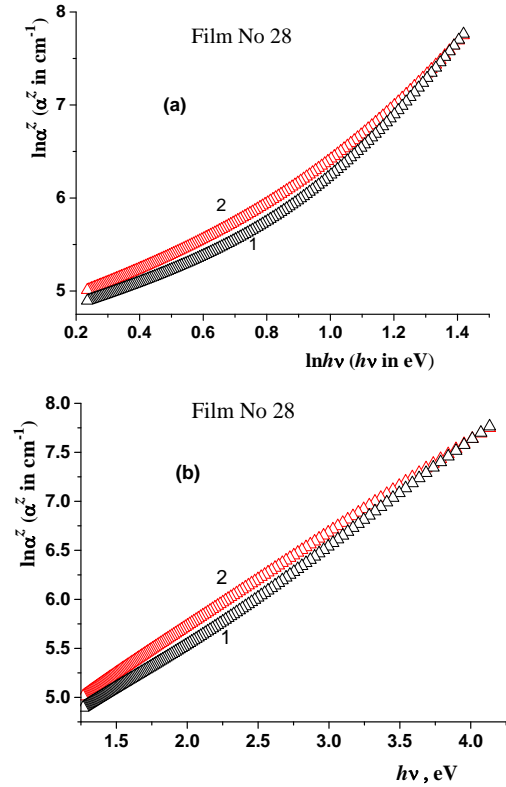


Fig. 6. α^z spectral dependences in $\ln \alpha^z - \ln h\nu$ (a) and $\ln \alpha^z - h\nu$ (b) coordinates for the as-deposited film 28 (1) and for the same film after one-hour annealing at 80°C in nitrogen atmosphere (2).

minimum values of α^z for the film 28 exhibits some decrease from 17.6 to 15.5 caused by annealing. Thus, the analysis of $\alpha(h\nu)$ plots for the films 16 and 28 by using the graphical representation technique shows direct correlation between the dynamic range of the extinction coefficient values and the ratio of the scattering and absorption contributions to the extinction coefficient – the wider this range the higher the α_s/α_a ratio.

The exact values of the parameters defining the absorption and scattering contribution can be obtained by minimization of G_2 . Nevertheless, the estimated values of the parameters characterizing absorption can be obtained through linear approximation of the plots presented in Fig. 6b. For the annealed film, the estimates of α_0 and E_U obtained using linear approximation of the entire set of 150 experimental points are $\alpha_0 = 45.3 \text{ cm}^{-1}$, $E_U = 1.045 \text{ eV}$. The slope of α^z experimental plot in the non-annealed film in $\ln \alpha^z - h\nu$ coordinates for $h\nu < 2.3 \text{ eV}$ is lower and for $h\nu > 2.7 \text{ eV}$ is higher than that in the annealed film. We used the range $h\nu \leq 2.25 \text{ eV}$ to estimate α_0^z and E_U for the as-prepared film. The linear approximation in this range produces $\alpha_0 = 43.86 \text{ cm}^{-1}$, $E_U = 1.135 \text{ eV}$. These estimates show that the absorption coefficient increases in its magnitude as a result of annealing, since both the increase in α_0 and the decrease in E_U tend to increase it. Thus, from the graphical analysis without an exact numerical solution of the inverse problem, the estimated

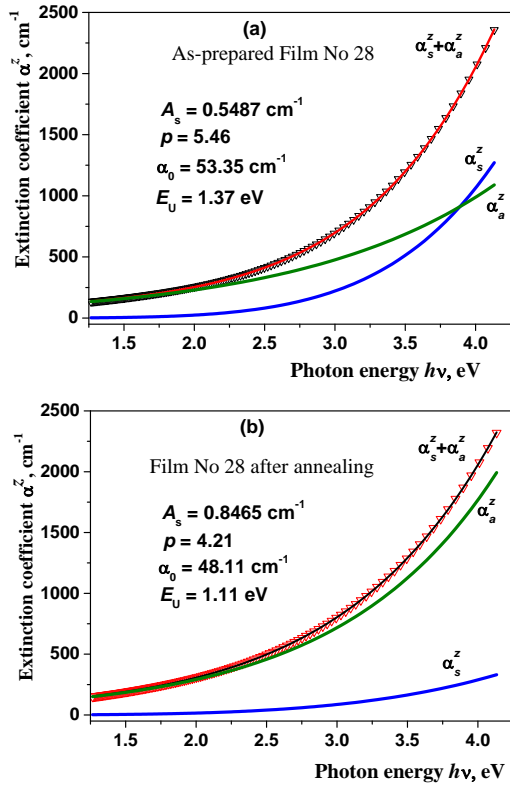


Fig. 7. α^z spectral dependence as well as its simulation with the sum of absorption (green curve α_a^z) and scattering (blue curve α_s^z) components for the film 28 before (a) and after (b) its one-hour annealing at 80 °C in nitrogen atmosphere.

values of the parameters α_0 and E_U are obtained, which are significant in themselves and are advisable to use as initial approximations when solving IP.

The results of IP solution are as follows. Before annealing, the minimum value is $G_2^{\min} = 2.1576 \cdot 10^2 \text{ cm}^{-2}$ and is reached at $\alpha_0 = 53.35 \text{ cm}^{-1}$, $E_U = 1.3703 \text{ eV}$, $A_s = 0.5487 \text{ cm}^{-1}$, $p = 5.46$. After annealing, the minimum value is $G_2^{\min} = 2.298 \cdot 10^2 \text{ cm}^{-2}$ and is reached at $\alpha_0 = 47.57 \text{ cm}^{-1}$, $E_U = 1.10 \text{ eV}$, $A_s = 0.8152 \text{ cm}^{-1}$, $p = 4.133$. As can be seen, the values of p and E_U obtained as a result of solving this IP in the annealed film are lower than that in the non-annealed one. It reinforces the conclusion obtained from the qualitative and quantitative graphical analysis of the $\alpha^z(h\nu)$ plots. As in the case of the horizontally polarized component (xy -polarization direction) for the vertically polarized component (z -polarization direction), the annealing leads to a decrease in scattering due to its transformation from ALS to Rayleigh-type scattering, as well as to the increase in the Urbach absorption. The increase in the α^z in relation to the α^{xy} in the as-deposited film 28 is more pronounced in the long-wave part of the spectrum – at $\lambda = 980 \text{ nm}$ $\alpha^z/\alpha^{xy} \cong 53.6$, at $\lambda = 300 \text{ nm}$ $\alpha^z/\alpha^{xy} \cong 2.61$. After annealing, the difference between these ratios becomes less pronounced: at $\lambda = 980 \text{ nm}$ $\alpha^z/\alpha^{xy} \cong 9.7$, at $\lambda = 300 \text{ nm}$ $\alpha^z/\alpha^{xy} \cong 2.1$.

4. Discussion

Polytetrafluoroethylene is a semi-crystalline polymer. The bulk PTFE was considered as a substance consisting of three phases: the crystalline, rigid amorphous and mobile amorphous ones [22, 23]. The strongly cross-linked material can be considered as the fourth phase. In bulk form the share of crystalline phase can reach 98% [22]; the refractive index of bulk PTFE is reported to be 1.4 [24]. Bulk PTFE has white appearance because of the high diffuse scattering caused by the quasi-crystalline structure. At the same time, physically deposited thin films can form fully amorphous polymers [24]. These films can have excellent adhesion to the substrate, good uniformity on the nanometer-level scale, a smooth surface, high transparency (unlike opaque bulk PTFE), and high hardness and elastic modulus superior to those of bulk PTFE [24, 25]. The $(-C_2F_4-)_n$ chains in crystalline regions are shorter and more tightly packed than that in amorphous regions. This results in lower density of PTFE in amorphous phase than that inherent to the quasi-crystalline one – the density of the pure amorphous and pure crystalline phases is 2.04 ± 0.01 and $2.30 \pm 0.01 \text{ g/cm}^3$, respectively [26]. Therefore, the change in density is an indication of the degree of crystallinity.

The values of the main parameters that demonstrate behavior of the scattering, absorption and refraction of light in the studied films are adduced in Table. Because the refractive index is related to the density of material, the refractive index of amorphous PTFE films is lower than that of bulk PTFE, and it is lower in the case of our films. Generally speaking, not only an increase in the proportion of amorphous phase but also the presence of porosity can contribute to the decrease in the refraction index of PTFE films. The same given value of the refractive index of a PTFE film can be obtained at different ratios of the volume fractions of the amorphous phase and pores – in this case, the smaller the fraction of the amorphous phase, the greater the porosity. In [9], the results of studying films 16 and 28 by using IR spectroscopy (IRS) are presented. They show that the (amorphous phase)/(crystalline phase) ratio for the film 16 is higher than in the film 28. This allows us to conclude that the lower value of the average refractive index $n^{av} = (2n^{xy} + n^z)/3$ of the film 16 is mainly caused not by its higher porosity, but by a higher content of the amorphous phase.

The IRS data from [9] also contain information about the spatial orientation of the chains. They show that, in the as-deposited films 16 and 28, a higher percentage of PTFE chains is predominantly aligned along the normal than in parallel to the substrate surface. Moreover, the proportion of predominantly vertically oriented chains is slightly higher in the film 28. This agrees with the larger birefringence in the film 28: $\Delta n = n^z - n^{xy}$ in the film 16 is 0.0027, while in the film 28 $\Delta n = 0.0098$. The relative intensity of the band located within the range 766...780 cm^{-1} , which serves as an

Table. The values of the main parameters that demonstrate behavior of scattering, absorption and refraction of light for the as-deposited films 16 and 28, as well as for the annealed film 28. Ordinary n^{xy} and extraordinary n^z refractive indexes as well as their difference $\Delta n = n^z - n^{xy}$ and average refractive index $n^{av} = (2n^{xy} + n^z)/3$ at $\lambda = 632.8$ nm. Scattering coefficients for the component of light polarized in the direction parallel α_s^{xy} and perpendicular α_s^z to substrate. Absorption coefficients for the component of light polarized in the direction parallel α_a^{xy} and perpendicular α_a^z to substrate. Urbach energy for the directions parallel E_U^{xy} and perpendicular E_U^z to substrate.

Film	No 16, as-deposited	No 28, as-deposited	No 28, annealed
n^{xy}	1.3496	1.3577	1.3436
n^z	1.3523	1.3675	1.3527
$\Delta n = n^z - n^{xy}$	0.0027	0.0098	0.0091
n^{av}	1.3505	1.3610	1.3466
Interval of α_s^{xy} (cm^{-1})	0.0223...8.27	2.5...900.0	9.47...826.1
p^{xy}	5.000	4.992	3.775
Interval of α_s^z (cm^{-1})	0.42...156.1	2.0...1271.6	2.3...331.2
p^z	4.833	5.46	4.21
Interval of α_a^{xy} (cm^{-1})	–	–	6.7...281.4
E_U^{xy} (eV)	–	–	0.767
Interval of α_a^z (cm^{-1})	0.28...9.77	134.3...1089.3	150.4...1992.7
E_U^z (eV)	0.720	1.37	1.11

indicator of the amorphous phase [27], in the annealed film 28 becomes equal to that in the as-prepared film 16 [9]. However, n^{av} of the film 28 is less than n^{av} of the film 16 (Table). This indicates that the annealed film 28 is more porous than the as-prepared film 16. Annealing of the film 28 leads also to an increase in the fraction of predominantly vertically oriented chains [9]. (Here it should be emphasized that in semi-crystalline polymers, where amorphous and crystalline regions are intimately related, the amorphous phases can have preferential aligning of polymer chains [23].) However, after annealing, Δn does not increase, but even slightly decreases from 0.0098 to 0.0091. This can be explained by an increase in the porosity of film 28 due to annealing, and possibly also by a change in mechanical stresses – the hardness and elastic modulus of film 28 sufficiently increase after annealing [9]).

As is well known, the Rayleigh-type scattering of isotropic materials is determined by the density fluctuations (fluctuations of refractive index). In calculating the light scattering from semi-crystalline polymeric materials, contributions both from the density (fluctuations in the mean refractive n^{av}) and orientation fluctuations have their impact on the results [28]. Theory of the Rayleigh scattering in anisotropic systems has been developed in [29]. It was shown that the Rayleigh ratio for vertically polarized light (z -polarization in our notation) is a function of refractive index anisotropy Δn and average refractive index n^{av} of the system. We believe that this is also true for self-organized structures, which are ensembles of the crystal and amorphous domains. ALS is inherent in precisely this kind of

structures. Thus, one can easily understand the stronger ALS in the as-deposited film 28 as compared to the as-deposited film 16. In the crystal phase, PTFE chains can arrange in fibrils with diameter of about 6 nm. These fibrils are collected in a rod-like structure [30]. Theory for light scattering from an assembly of anisotropic rods has been developed in [31]. It was shown that the scattered intensity depends not only on the magnitude of the anisotropy of the system, but also on the value of the ordinary refractive index. This theory successfully explained the scattering patterns of oriented (stretched) and un-oriented (non-stretched) thick semi-crystalline PTFE films. Being based on this theory, the decrease in the value of α_s in the film 28 due to annealing can be primarily explained specifically by the decrease in n^{xy} .

As it is seen from Figs 3, 5, 7 and Table, in the as-deposited films only the component of light polarized along the normal to substrate undergoes absorption. Thus, the defects responsible for the Urbach absorption have an anisotropic structure and their transition dipole moments are oriented strictly along the normal to the substrate. For this direction of polarization, there is a direct correlation between scattering's and subband absorption's coefficients – the larger the scattering coefficient, the larger the absorption one. This shows that the defects are located in or near scatterers that, obviously, have an anisotropic form. The scattering is anomalous, *i.e.*, it is due to the interference effects caused by correlated spatial arrangement of the scatterers. In this case, the scatterers have low bulk concentration, their size is less than the light wavelength and their relative refractive index (relative to “matrix”) is close to unity

[3, 32]. The destruction of this ordered arrangement of anisotropic scatterers in the film 28 as a result of annealing causes a significant (several times) decrease in scattering for the z -polarization direction. This is accompanied by an increase in absorption, which is especially significant for the xy -polarization directions. Thus, as a result of annealing, the degree of dichroism α_a^z/α_a^{xy} decreases. This parameter does not demonstrate a clear correlation either with the value of Δn or with the degree of vertical ordering of chains in domains. But it shows a clear correlation with the exponent p . This suggests that scatterers and defects are located mainly in the interface regions of domains formed as a result of the self-organization processes during film deposition.

5. Conclusion remarks

We used uniaxially anisotropic polytetrafluoroethylene films as a medium for studying the separation of the scattering and defect (Urbach) absorption contributions to the extinction/attenuation coefficient. These films have different spectral dependences of ordinary α^{xy} and extraordinary α^z extinction coefficients beyond the fundamental absorption edge. Qualitative, semi-quantitative and quantitative analysis was performed using the graphical representation technique. This graphical approach is useful for the initial express assessment of scattering and absorption contributions. For this, a comparative qualitative analysis of the experimental dependences $\alpha(h\nu)$ plotted in semi-logarithmic $\ln\alpha - h\nu$ and double logarithmic $\ln\alpha - \ln h\nu$ coordinates should be performed. Quantitative estimates of the values of the parameters characterizing the wavelength-dependent and independent scattering, as well as subband absorption, are determined by graphical linear approximation of the extinction coefficient spectral plots in $\ln\alpha - \ln h\nu$, $\alpha - (h\nu)^p$, $\ln\alpha - h\nu$ coordinates. In the cases of considerable contributions of all components to the extinction coefficient, the most accurate values of the scattering and absorption parameters can only be obtained by minimizing the goal functions G_2 , G_3 . But even in this case, a carefully performed preliminary graphical analysis is extremely important. It allows one to narrow the search range of the model parameter values when solving the inverse problem, which not only accelerates the search for the absolute minimum but also prevents falling into possible false minima. Analysis of possible causes for observed spectral behavior of the scattering and absorption coefficients of PTFE films in the “transparency range” of the material enables to obtain additional information regarding the film structure at different levels of its organization.

References

1. Bauer J., Gutke M., Heinrich F. *et al.* Novel UV-transparent 2-component polyurethane resin for chip-on-board LED microlenses. *Opt. Mater. Express*. 2020. **10**, No 9. P. 2085–2099. <https://doi.org/10.1364/OME.393844>.
2. Bauer J., Fursenko O., Heinrich F. *et al.* Determination of optical constants and scattering properties of transparent polymers for use in optoelectronics. *Opt. Mater. Express*. 2022. **12**, No 1. P. 204–224. <https://doi.org/10.1364/OME.434715>.
3. Shepilov M.P., Dymshits O.S., Zhilin A.A. Light scattering in glass-ceramics: revision of the concept. *J. Opt. Soc. Am. B*. 2018. **35**, No 7. P. 1717–1724. <https://doi.org/10.1364/JOSAB.35.001717>.
4. Dunch T., Jackson S. Rayleigh scattering with material dispersion for low volume fraction transparent glass ceramics. *Opt. Mater. Express*. 2022. **12**, No 7. P. 2595–2608. <https://doi.org/10.1364/OME.457319>.
5. Gritsenko K.P. Vacuum-evaporation deposited polytetrafluoroethylene films: Growth mechanism, properties and applications of vacuum-deposited PTFE films. *Russ. J. Gen. Chem.* 2009. **79**, No 3. P. 642–656. <https://doi.org/10.1134/S1070363209030463>.
6. Dake S., Rajopadhye N., Bhoraskar S. Evaluation and characterisation of chemically modified polymers as secondary electron emitters. *J. Phys. D: Appl. Phys.* 1987. **20**, No 12. P. 1631–1636. <https://doi.org/10.1088/0022-3727/20/12/014>.
7. Seki K., Tanaka H., Ohta T. *et al.* Electronic structure of poly (tetrafluoroethylene) studied by UPS, VUV absorption, and band calculations. *Phys. Scr.* 1990. **41**, No 1. P. 167–171. <https://doi.org/10.1088/0031-8949/41/1/041>.
8. Fatti G., Righi M.C., Dini D., and Ciniero A. First-principles insights into the structural and electronic properties of PTFE in its high-pressure phase (Form III). *J. Phys. Chem. C*. 2019. **123**, No 10. P. 6250–6255. <https://doi.org/10.1021/acs.jpcc.8b11631>.
9. Grytsenko K., Kolomzarov Yu., Lytvyn P. *et al.* Optical and mechanical properties of thin PTFE films, deposited from a gas phase. *Macromol. Mater. Eng.* 2023. **308**, No 6. P. 2200617. <https://doi.org/10.1002/mame.202200617>.
10. Stengel D., Calori G.M., Giannoudis P.V. Graphical data presentation. *Injury*. 2008. **39**, No 6. P. 659–665. <https://doi.org/10.1016/j.injury.2008.01.050>.
11. Grytsenko K., Ksianzou V., Kolomsarov Yu. *et al.* Fluoropolymer film formation by electron activated vacuum deposition. *Surface*. 2021. **4**, No 1. P. 66–80. <https://doi.org/10.3390/surfaces4010009>.
12. Sopinskyy M.V., Vlasenko N.A., Lisovskyy I.P. *et al.* Formation of nanocomposites by oxidizing annealing of SiO_x and $\text{SiO}_x(\text{Er},\text{F})$ films: Ellipsometry and FTIR analysis. *Nanoscale Res. Lett.* 2015. **10**. Art. No 232. <https://doi.org/10.1186/s11671-015-0933-0>.
13. Sopinskii N.V. Determination of optical constants of a biaxially anisotropic film by standard multiangle monochromatic ellipsometry. *Opt. Spectrosc.* 2017. **123**, No 5. P. 778–782. <https://doi.org/10.1134/S0030400X17110212>.
14. Gartner M., Stoica M., Nicolescu M., Stroescu H. The ellipsometry versatility in the study of sol-gel films. *J. Sol-Gel. Sci. Technol.* 2021. **98**, No 1. P. 1–23. <https://doi.org/10.1007/s10971-021-05504-2>.

15. Sopinsky M.V., Ol'khovik G.P. Generalized null-ellipsometry in the Polarizer–Sample–Analyzer scheme. *Opt. Spectrosc.* 2022. **130**, No 2. P. 92–101. <https://doi.org/10.1134/S0030400X22010155>.
16. Shepilov M. Anomalous light scattering in nanostructured glasses formed by simultaneous nucleation and diffusion-limited growth of particles: Modeling. *J. Non-Cryst. Solids.* 2023. **600**. Art. No 121958. <https://doi.org/10.1016/j.jnoncrysol.2022.121958>.
17. Berthier T., Fokin V.M., Zanotto E.D. New large grain, highly crystalline, transparent glass-ceramics. *J. Non-Cryst. Solids.* 2008. **354**. P. 1721–1730. <https://doi.org/10.1016/j.jnoncrysol.2007.08.052>.
18. Jaglarz J., Dulian P., Karasinski P., Winkowski P. Scattering phenomena in porous sol-gel-derived silica films. *Coatings.* 2020. **10**, No 6. Art. No 509. <https://doi.org/10.3390/coatings10060509>.
19. Studenyak I., Kranjec M., Kurik M. Urbach rule in solid state physics. *Int. J. Opt. Appl.* 2014. **4**, No 3. P. 76–83. <http://doi.org/10.5923/j.optics.20140403.02>.
20. Sakaguchi S., Todoroki S.-I. Optical properties of GeO₂ glass and optical fibers. *Appl. Opt.* 1997. **36**, No 27. P. 6809–6814. <https://doi.org/10.1364/AO.36.006809>.
21. Busse L.E., McCabe G.H., Aggarwal I.D. Wavelength dependence of the scattering loss in fluoride optical fibers. *Opt. Lett.* 1990. **15**, No 8. P. 423–424. <https://doi.org/10.1364/OL.15.000423>.
22. Calleja G., Jourdan A., Ameduri B., Habas J.-P. Where is the glass transition temperature of poly(tetrafluoroethylene)? A new approach by dynamic rheometry and mechanical tests. *Eur. Polym. J.* 2013. **49**, No 8. P. 2214–2222. <https://doi.org/10.1016/j.eurpolymj.2013.04.028>. hal-00844535.
23. Wietzke S., Jansen C., Reuter M. *et al.* Thermomorphological study of the terahertz lattice modes in polyvinylidene fluoride and high-density polyethylene. *Appl. Phys. Lett.* 2010. **97**, No 2. Art. No 022901. <https://doi.org/10.1063/1.3462312>.
24. Cho E., Song S., Kim M. *et al.* Investigation of thermal property of plasma-polymerized fluorocarbon thin films. *Polym. Adv. Technol.* 2022. **33**, No 10. P. 3470–3478. <https://doi.org/10.1002/pat.5800>.
25. Kang T.W., Kim S.H., Kim M., Cho E., Lee S.J. Highly flexible, hydrophobic, and large area plasma-polymer-fluorocarbon/Cu/SiN_x transparent thin film heater and thermotherapy pad application. *Plasma Process. Polym.* 2020. **17**, No 4. Art. No 1900188. <https://doi.org/10.1002/ppap.201900188>.
26. Yassien K.M., Agour M., El-Bakary M.A. Determination of physical properties of irradiated PTFE fibers using digital holographic microscopy. *Appl. Phys. B.* 2019. **125**. Art. No 180. <https://doi.org/10.1007/s00340-019-7291-z>.
27. Starkweather H.W., Jr., Ferguson R.C., Chase D.B., Minor J.M. Infrared spectra of amorphous and crystalline poly(tetrafluoroethylene). *Macromolecules.* 1985. **18**, No 9. P. 1684–1686. <https://doi.org/10.1021/ma00151a007>.
28. Koberstein J., Russell T.P., Stein R.S. Total integrated light-scattering intensity from polymeric solids. *J. Polym. Sci.: Polym. Phys. Ed.* 1979. **17**, No 10. P. 1719–1730. <https://doi.org/10.1002/pol.1979.180171008>.
29. Norris F.H. and Stein R.S. The scattering of light from thin polymer films. IV. Scattering from oriented polymers. *J. Polym. Sci.: Polym. Phys. Ed.* 1958. **27**, No 115. P. 87–114. <https://doi.org/10.1002/pol.1958.1202711508>.
30. Puts G.J., Crouse P., Ameduri B.M. Polytetrafluoroethylene: Synthesis and characterization of the original extreme polymer. *Chem. Rev.* 2019. **119**, No 3. P. 1763–1805. <https://doi.org/10.1021/acs.chemrev.8b00458>.
31. Rhodes M.B., Stein R.S. Scattering of light from assemblies of oriented rods. *J. Polym. Sci. Pt A-2: Polym. Phys. Ed.* 1969. **7**, No 9. P. 1539–1558. <https://doi.org/10.1002/pol.1969.160070909>.
32. Berdnik V.V., Loiko V.A. Light scattering by ensemble of non-absorbing correlated two-layered particles: specific feature for spectral dependence of extinction coefficient. *Appl. Opt.* 2011. **50**, No 22. P. 4246–4251. <https://doi.org/10.1364/AO.50.004246>.

Authors and CV



Mykola V. Sopinsky, born in 1957, Senior researcher at the V. Lashkaryov Institute of Semiconductor Physics, NAS of Ukraine. He defended his Ph.D. thesis in Solid State Physics in 1996. Authored over 150 publications. The area of his scientific interests includes interference lithography, photo- and thermostimulated processes in thin-film structures, plasmonics, synthesis and characterization of nanomaterials, ellipsometry. <http://orcid.org/0000-0002-0101-1241>



Claus Villringer, born in 1983, Ph.D. researcher in the Photonics and Optical Technologies group at Technical University of Applied Sciences Wildau (TH Wildau), Germany. He received his B.S. degree in physical engineering from the University of Applied Sciences Ravensburg-Weingarten, Germany and his M.Eng. degree in photonics from the Technical University of Applied Sciences Wildau, Germany. Claus Villringer is coauthor of 16 publications. The area of his main research interests includes thin-film technology, spectroscopic ellipsometry, the development of tunable Fabry-Pérot sensors for parallelized photoacoustic signal acquisition. E-mail: villringer@th-wildau.de, <https://orcid.org/0000-0001-5158-2424>



Kostyantyn P. Grytsenko, born in 1957, Senior Researcher at the V. Lashkaryov Institute of Semiconductor Physics, NASU. He defended his Ph.D. in 1997. Authored 65 journal papers, 120 conference reports, and 9 patents. The area of his scientific interests includes soft condensed matter and its application in photonics, information recording, sensorics. E-mail: d.grytsenko@gmail.com, <https://orcid.org/0000-0002-2956-3654>



Yuriy V. Kolomzarov, born in 1963, Senior researcher at the V. Lashkaryov Institute of Semiconductor Physics, NAS of Ukraine. He defended his Ph.D. thesis in Technical Sciences in 2005. He is the author of more than 100 publications and 20 patents. His main research activity is in the

field of technology for deposition of amorphous hydrogenated silicon for high efficiency solar cells and technology of thin film organic-inorganic light-emitting heterostructures. E-mail: kolomzarov@isp.kiev.ua, <http://orcid.org/0000-0002-6314-9529>



Sigurd Schrader, born in 1952, Full Professor for Photonics and Optical Technologies at Technical University of Applied Sciences Wildau, Germany. He defended his Ph.D. thesis at the Institute of Organic Chemistry of Academy of Sciences

of the German Democratic Republic, Berlin, Germany in 1983. Since 2019 Prof. Schrader is Director of the Institute of Applied Physics, Technical University of Applied Sciences Wildau, Germany. The area of his scientific interests includes photonics, optical technologies, plasma technology, laser spectroscopy, laser processing, organic and inorganic semiconductors, organic electronics and photonics, soft matter, polymer sciences. His publications include 10 book chapters, 150 publications in international refereed journals, 80 invited lectures at international conferences, 15 patents and patent applications.

E-mail: sigurd.schrader@th-wildau.de, <https://orcid.org/0000-0002-9943-4727>

Authors' contributions

Sopinsky M.V.: conceptualization, methodology, modeling, visualization, writing – original draft, writing – review & editing.

Grytsenko K.P.: conceptualization, data curation, formal analysis, writing – review & editing.

Villringer C.: ellipsometry investigation, visualization.

Kolomzarov Yu.V.: deposition methods, deposition of samples for research.

Schrader S.: conceptualization, resources, writing – review & editing.

Визначення внесків розсіювання та урбахівського поглинання в коефіцієнт екстинкції світла в плівках ПТФЕ методом графічного представлення та чисельним розв'язанням оберненої задачі

М.В. Сопінський, К.П. Гриценко, С. Villringer, Ю.В. Коломзаров, S. Schrader

Анотація. Проаналізовано еліпсометрично отримані спектральні залежності звичайного α^{xy} та незвичайного α^z коефіцієнтів екстинкції/ослаблення в спектральному діапазоні $\lambda = 300 \dots 980$ нм одночасно анізотропних політетрафторетиленових (ПТФЕ) плівок. Розглянуто можливості та особливості техніки графічного представлення для визначення внеску релєївського розсіювання та урбахівського поглинання в коефіцієнт ослаблення світла в спектральному діапазоні за межами краю фундаментального поглинання. Показано, що залежно від ситуації графічний підхід дає змогу оцінити ці внески якісно, напівкількісно чи кількісно. Висновки, зроблені за допомогою аналізу техніки графічного зображення, підтверджуються чисельним розв'язанням оберненої задачі шляхом моделювання експериментальних залежностей $\alpha^{xy}(\lambda)$, $\alpha^z(\lambda)$ в рамках процедури найкращої відповідності. За допомогою обох цих підходів було встановлено, що в осаджених плівках ПТФЕ має місце так зване аномальне розсіювання світла (ALS) зі спектральною залежністю коефіцієнта розсіювання $\alpha_s \approx a_s \lambda^{-p}$ ($p > 4$). Трансформація аномального розсіювання в релєївське з $p \cong 4$ внаслідок віддалу супроводжується збільшенням урбахівського (підзонного) поглинання. Обидва ці фактори викликають звуження динамічного діапазону значень коефіцієнта екстинкції. Коефіцієнти розсіювання та поглинання більші для компоненти світла, поляризованої в напрямку перпендикулярному до підкладки, порівняно з компонентою, поляризованою у напрямку паралельному до підкладки. Обговорюється зв'язок між спостережуваною поведінкою коефіцієнтів розсіювання і поглинання та структурою плівок.

Ключові слова: релєївське розсіювання, хвіст Урбаха, коефіцієнт поглинання, коефіцієнт розсіювання, графічний метод, еліпсометрія, політетрафторетилен.